

Efficient water desalination using Bernoulli effect

Tianzhen Wang^{a,†}, Lu Huang^{b,†}, Junxian Pei^c, Xuejiao Hu^a, Haifeng Jiang^{a,*}

^aKey Laboratory of Hydraulic Machinery Transients (Wuhan University), Ministry of Education, School of Power and Mechanical Engineering, Wuhan University, Wuhan, Hubei 430072, China, emails: hfjiang@whu.edu.cn (H. Jiang), 2015102080027@whu.edu.cn (T. Wang), xjhu@whu.edu.cn (X. Hu)

^bSchool of Mechanical and Electrical Engineering, Wuhan Institute of Technology, Wuhan, Hubei 430205, China, email: luhuang@wit.edu.cn (L. Huang)

^cCollege of Water Resource and Hydropower, Sichuan University, Chengdu 610065, China, email: jxpei@scu.edu.cn (J. Pei)

Received 11 March 2022; Accepted 15 August 2022

ABSTRACT

Due to the Bernoulli effect, the directional flow of water molecules on one side of the nanopore will produce a pressure drop compared with the fluid on the other side, which makes the water molecules on the static brine side be pumped through the slit with salt ions being blocked. A high water flux of 857 L/m²/h·bar with 100% salt rejection rate can be obtained in a single-layer graphene membrane with the slit of 0.7 nm under an external pressure of 250 MPa. This work provides a novel desalination method and a useful guideline for the future development of new pumping systems that separate ions or molecules.

Keywords: Graphene; Water desalination; Bernoulli effect; Nanofluidics; Molecular dynamics simulation

1. Introduction

The shortage of fresh water threatens the survival of humans and other species on the earth. At least 4 billion people (two-thirds of the world's population) face severe water shortages [1–5]. As is well known, approximately 71% of the earth's surface is covered by water, but about 97% of these water resources are mainly distributed in the ocean. The thermal desalination method that uses waste heat to drive the phase change of water and the widely used permeable membrane-based desalination method have become effective ways to obtain fresh water from the ocean [6–8]. However, these methods have suffered from some obvious shortcomings. For example, the multi-stage flash evaporation (MSF) has complex equipment, high cost and low efficiency [9,10]. Meanwhile, corrosion of materials would occur frequently and pollute fresh water [11,12]. On the other hand, reverse osmosis (RO) has the

disadvantages of higher energy consumption and membrane fouling [13–15]. Therefore, how to obtain freshwater resources efficiently and economically is a worldwide problem that needs to be solved.

Graphene-based membrane is considered as a nano-material with great potential for desalination [16–20] and ion separation [21–25] due to its high chemical stability, excellent mechanical strength, controllable pore size, and atomic thickness. Nguyen and Beskok [26] simulated the seawater desalination across a single-layer graphene with positive and negative charged nanopores driven by pressure, and believed that charged nanoporous graphene have great potential as reverse osmosis membrane. Willcox and Kim [27] dislocated graphene to form a tortuous channel and studied the effect of layer spacing on the structure and kinetics of water in graphene oxide membranes. Besides, Li et al. [28] studied the mechanism of molecule transport in the two-dimensional nanochannels of graphene oxide

* Corresponding author.

† These authors contributed equally to this work.

by simulation, and found that the strong electrostatic, van der Waals (vdW) and hydrogen bond interactions from oxygen-containing groups largely hinder the transport of water and ions.

In this manuscript, a new desalination method is proposed by combining nanomaterials and the Bernoulli effect, and it is proved that the Bernoulli effect can be used for desalination at the nanoscale. We first proposed a desalination model using Bernoulli effect, and then studied the effects of different slit sizes and the number of graphene layers on desalination performance, and finally compared it with other literatures to evaluate the economy and development prospects of the desalination model.

2. Simulation method and theory

The mechanical energy of flowing fluid possesses components of kinetic energy, gravitational potential energy, and pressure potential energy. The essence of Bernoulli effect is the conservation of fluid mechanical energy, that is, the local pressure of fluid would decrease when flow rate increases at the same height. Bernoulli effect could be described as:

$$p + \frac{1}{2}\rho v^2 + \rho gh = \text{const} \quad (1)$$

where p is the local pressure of fluid, v is the local velocity, ρ is the local density, g is the acceleration of gravity, h is the height, and const is a constant. Notably, the formula is suitable for incompressible fluids with negligible viscosity and steady flow.

Water flux and salt rejection rate for different slit sizes and graphene layers were simulated with models as shown in Fig. 1. Force exerted on each water molecule in the yellow area drives the water to flow from left to the right in upper reservoir. In order to improve calculation efficiency and distinguish simulation results, the external forces F are set as 0.0268, 0.0402, 0.0536, and 0.067 kcal/mol·Å respectively, corresponding to external pressures of 100, 150, 200, and 250 MPa. The pressures we used in the simulation are higher than that in reality, which is to improve the computational efficiency and obtain the results under harsh conditions [29–31]. In order to simplify the calculation process and highlight the mechanism of Bernoulli effect in desalination, no functional groups are added to the surface of graphene, the charge of the carbon atoms of graphene are neutral, and the electrochemical effect of the interface is not considered, which is a usual practice in the molecular dynamics simulation literature [32,33].

All MD simulations in this work were performed by large-scale atomic/molecular massively parallel simulator (LAMMPS) [36], using Nosé–Hoover thermostat to maintain the system temperature at 293.15 K [37,38]. Periodic boundary conditions are applied in all directions with a free space above the water surfaces in both reservoirs. Water molecules are described by the four-point transferable intermolecular potential (TIP4P) model [39]. The SHAKE algorithm [40] is implemented to keep the O–H bond and H–O–H angle fixed at the equilibrium values of 0.9572 Å and 104.52°, respectively. The non-bonded interactions

between water molecules, ions, and carbon atoms are calculated using 12–6 Lennard–Jones (LJ) and Coulomb potentials, with a cut-off radius of 10 Å for both interactions. The Lennard–Jones parameters of different atoms are estimated according to the Lorentz–Berthelot combination rules described as $\sigma_{ij} = (\sigma_{ii} + \sigma_{jj})/2$ and $\epsilon_{ij} = \sqrt{\epsilon_{ii}\epsilon_{jj}}$ [41]. In addition, the particle-particle-particle-mesh (PPPM) solver has a relative accuracy of 0.0001, which is used to deal with long-range electrostatic interactions between charged particles [42]. The Lennard–Jones parameters and charges of species are presented in Table 1.

Water flux in this simulation is defined as the number of water molecules passing through the membrane per unit time. Salt rejection rate is the ratio of ions left in the static reservoir when half of water molecules in the reservoir pass through the membrane to the original total ions number, which is defined as:

$$D = \frac{N_{1/2}}{N} \quad (2)$$

where D is the salt rejection rate, N is the number of ions in the lower reservoir at the beginning, and $N_{1/2}$ is the number of remaining ions in the static reservoir when half of water molecules in the reservoir pass through the membrane.

3. Results and discussion

Fig. 2 shows the volume changes on both sides of the single-layer graphene with a 0.7 nm slit under external pressure of 200 MPa. As the simulation progresses, the volume of water in the static reservoir gradually reduces, while the dynamic reservoir gradually increases, indicating a net water flow through the membrane slit. The number variations of water molecules in the dynamic and static reservoirs are shown in Fig. 3a and b. As can be seen from the figures, when the slit size of single-layer graphene is 0.7 nm, as the external force increases, the water flux increases accordingly. The same trends were also observed for slits of 0.6, 0.8, and 0.9 nm, as shown in Figs. S1, S3, S5. The velocity components of water molecules in the x and z -directions are further calculated to provide an insight into the detail of flow through the slit. As the external force increases, v_x of water in the dynamic reservoir increase accordingly (Fig. 3d), resulting the same trend for v_z of water in the slit (Fig. 3c). Velocities of water for the single-layer graphene with slits of 0.6, 0.8, and 0.9 nm can be seen in Figs. S2, S4, S6, respectively, showing the similar tendency.

Table 1
Lennard–Jones parameters and charges of species [34,35]

q (e)	ϵ (kcal/mol)	σ (Å)	Atom	Type
−0.8476	0.1553	3.169	O	Water
+0.4238	0	0	H	Water
0	0.105	3.851	C	Graphene
1	0.0469	2.430	Na	Ion
−1	0.146	4.402	Cl	Ion

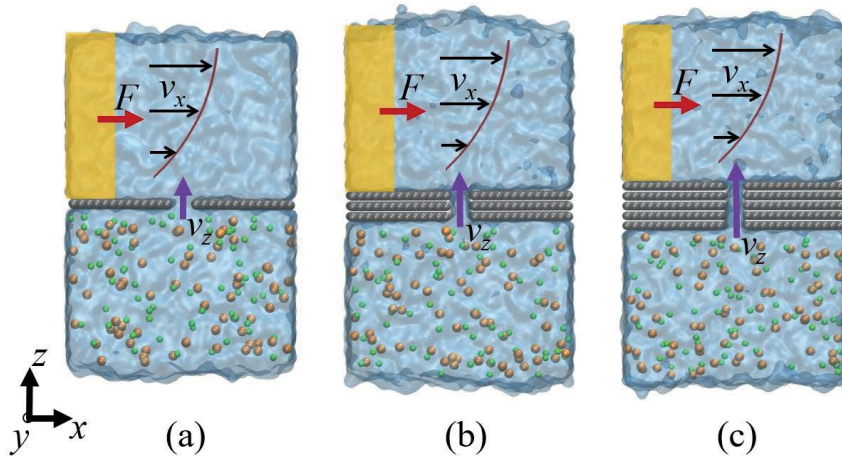


Fig. 1. Models for desalination using Bernoulli effect with the upper reservoir of pure water and the lower reservoir of 0.6 mol/L NaCl solution separated by the middle graphene of (a) single-layer, (b) three-layer, and (c) five-layer, respectively. The water molecules in the yellow area are applied with external force in the direction indicated by red arrow to simulate external pressure. Gray spheres represent graphene, blue spheres represent water, orange spheres represent sodium ions, and green spheres represent chloride.

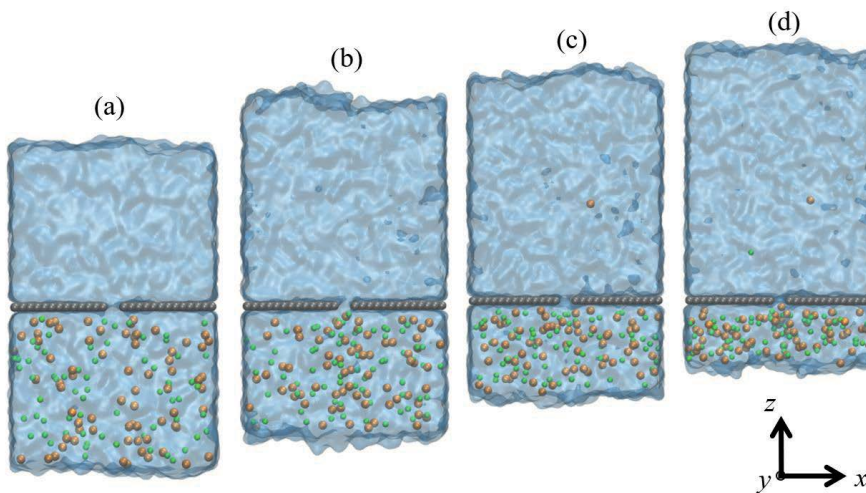


Fig. 2. Snapshots of volume change for single-layer graphene with a 0.7 nm slit under 250 MPa at (a) 0 ns, (b) 1.5 ns, (c) 3.0 ns, and (d) 4.5 ns. Gray spheres represent graphene, blue spheres represent water, orange spheres represent sodium ions, and green spheres represent chloride.

In order to better understand the desalination process using Bernoulli effect, the water density is analyzed. Fig. 4a shows the density at different positions on both sides of the single-layer membrane. Fig. 4b displays the density in the static reservoir (black lines) and the dynamic reservoir (lines of other colors) vs. the simulation time and external pressure. It can be seen that the water density in the dynamic reservoir fluctuates with the simulation time and external pressures. The time-average values are marked with the dotted lines. By using the linear relationship between density and pressure [43]: $\left(\frac{\partial \rho}{\partial p}\right)_T \cong 5.9 \times 10^{-4} \text{ g/MPa}\cdot\text{cm}^3$, the pressures converted from the different water densities in the dynamic reservoir and the static reservoir are shown in Table 2. If the pressure in the static reservoir is set to 0 MPa, the pressure in dynamic

reservoir would be a negative value and further decrease as the external force increases. According to the Bernoulli effect as Eq. (1), the kinetic energy and pressure potential in the dynamic reservoir are converted to each other, so a faster flow rate above the slit causes an increase in the pressure drop. Under the action of this pressure difference, the water is pressed from the static reservoir to the dynamic reservoir, and the salt rejection effect is achieved under the barrier of the slit.

The desalination performances of single-layer membranes with different slits under various external forces are compared in Fig. 5. It is clear that the water flux increases with the increase of slit sizes and external forces, but the salt rejection rate is significantly affected by slit sizes while basically not affected by external forces. The salt rejection rate of single-layer membrane with a slit of 0.6 nm or 0.7 nm

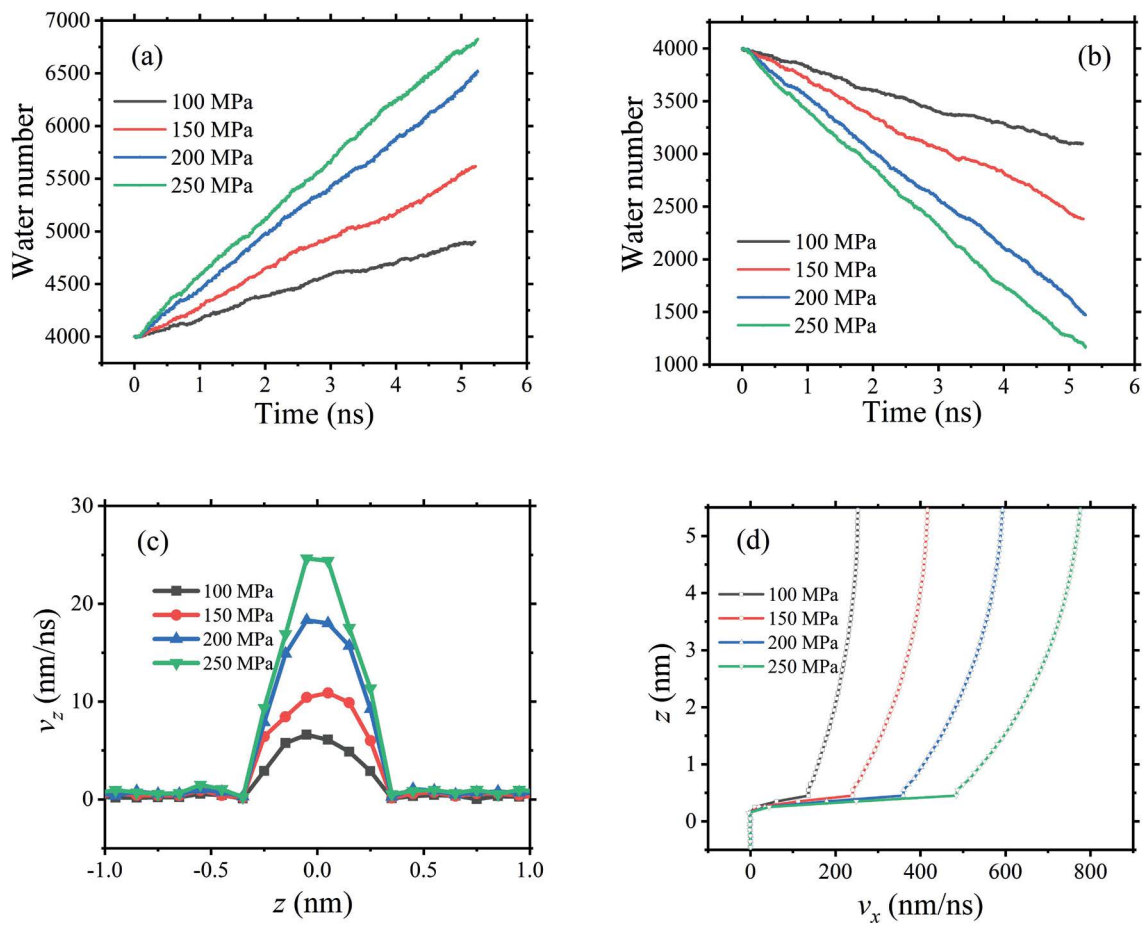


Fig. 3. Number variation of water molecules in (a) the upper dynamic reservoir and (b) the lower static reservoir under different external force for single-layer graphene with a 0.7 nm slit. The velocity component of water molecules in the (c) z-direction and (d) x-direction along z-axis for the single-layer graphene with a 0.7 nm slit.

Table 2
Conversion of different water densities to pressures

External pressure (MPa)	0	100	150	200	250
Water density (g/cm^3)	0.947	0.933	0.924	0.912	0.896
Pressure in reservoir (MPa)	0	-23.7	-39.0	-59.3	-86.4

was very close to 100%. The equilibrium vdW distance $\sigma_{\text{C-O}}$ between the carbon atoms at the edge of slit and oxygen atom in water molecules is 3.508 Å, which makes it difficult for water molecules to pass through a slit of 0.6 nm but smoothly for 0.7 nm. On the other hand, the ions of Na^+ and Cl^- with hydration radii of 3.25 and 3.80 Å, respectively [44], would be blocked by both the slits of 0.6 and 0.7 nm, but the former is more obviously [45].

The desalination performances of multi-layer graphene with slit of 0.8 and 0.9 nm were further studied. We did not study the cases of 0.6 and 0.7 nm, because the water flux of single-layer membrane with a slit of 0.6 nm is already very small. In addition, increasing the number of layers would not have a beneficial effect on water flux. Meanwhile, the salt rejection rate of the single-layer membrane with a slit of

0.7 nm is very close to 100%, and increasing the number of layers of the membrane has no more room for improvement in the salt rejection rate. As shown in Fig. 1, three-layer or five-layer graphene is used to construct multilayer membranes. In three-layer or five-layer membrane, the number changes of water molecules in the upper dynamic reservoir and the lower static reservoir with the simulation time and different external forces can be seen from Figs. S7, S9, S11, S13. Along the z-axis in the model, the velocity component of water molecules in the z-direction and the x-direction can be seen from Figs. S8, S10, S12, S14. The water flux and salt rejection rate of single-layer, three-layer or five-layer membrane with slits of 0.8 and 0.9 nm are all displayed in Fig. 6. As can be seen in the figure, the water flux increases with the external force but decreases with the number of layers.

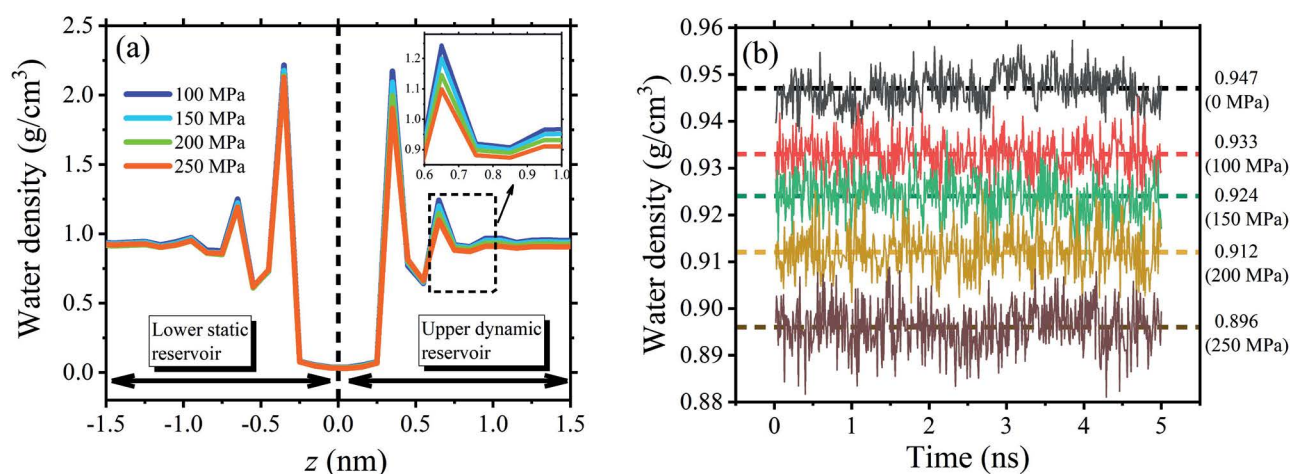


Fig. 4. Density profiles of water molecules changes with (a) position along z -axis and (b) simulation time under different external force for the single-layer graphene with a 0.7 nm slit. The dotted lines are the time average of the water density under different external pressures.

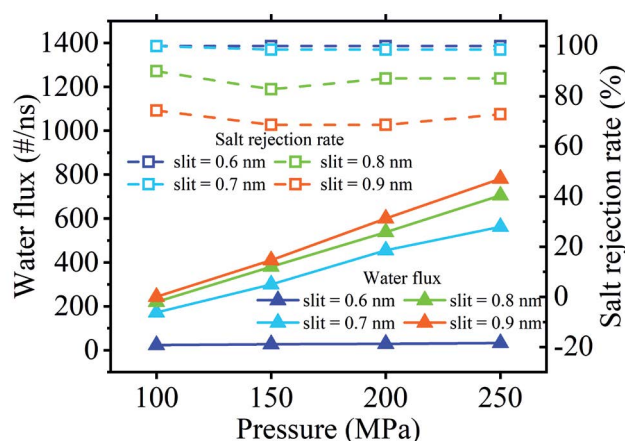


Fig. 5. Water flux and salt rejection rate changes with external force and slit size for single-layer graphene.

Due to size effect, the salt rejection rate of membranes with a slit of 0.8 nm is higher than that of membranes with a slit of 0.9 nm. Similar to the single-layer graphene, the slit size rather than external force is the key factor in controlling the salt rejection rate and the water flux is affected by both of the external pressures and the slit size.

According to the results discussed above, we suggest that it need to comprehensively consider all factors such as slits, external forces, and membrane thickness to achieve a higher water flux with the premise of higher salt rejection rate. Increasing the size of slits on membrane is beneficial to improve water flux but not conducive to the salt rejection rate. The increase in the number of layers can increase the salt rejection rate, but this is achieved at the cost of reducing the water flux. In addition, increasing the external force as much as possible in consideration of the membrane bearing capacity can increase the water flux.

As shown in Table 3, the simulated calculation results of this work are compared with commercial RO [46], two-stage RO model simulation [47], 25% cellulose acetate

(CA) + 0.05% carbon nanotubes (CNT) membranes [48], graphene oxide (GO) modified polyamide reverse osmosis (RO) membrane [49], thin-film nanocomposite (TFN) membranes fabricated by embedding graphene oxide quantum dots/silver phosphate (GOQD/AP) into polyamide (PA) layers [50], graphitic carbon nitride ($g\text{-C}_3\text{N}_4$) [51], graphene strips woven filter membrane (GWFM) [52], the bilayer graphene (BGR) membranes with ripples [53]. Compared with literatures, it can be seen that when the desalination rate is 100% the water flux is similar to the value of molecular dynamics simulation in literatures, and significantly higher than the value of RO.

We calculated the energy consumption by using Eq. (3).

$$E = \frac{F\bar{v}_x}{u_z N_A} \quad (3)$$

where E is the energy consumption per ton, kWh/t; F is the force exerted on water molecules, $\text{J/mol}\cdot\text{\AA}$; \bar{v}_x is average velocity driven by external pressure paralleled to the membrane, nm/ns; u_z is the water flux across the membrane, t/s; N_A is the Avogadro constant.

As shown in Fig. 7, when the external pressures are 100, 150, 200 and 250 MPa, respectively, the energy consumption per ton with different slits is calculated. We find that the relationship between energy consumption and external pressure is linear, similar to the linear relationship between external pressure and water flux [18,54]. After the linear fitting of external pressure and energy consumption, the energy consumption value can be obtained on the fitting line by using the feed water pressure of commercial RO, it can be inferred that when the external pressure takes the pressure value used by commercial RO, the value of energy consumption per ton in this work using the Bernoulli effect is not significantly higher than the energy consumption of commercial RO reported in the literature [55–58].

Carbon based nanomaterials have much smoother surface and small pore size, so can reduce the chances of heterogeneous nucleation on the surface, and prohibit

Table 3
Comparison with literatures

	Water flux (L/(m ² ·h·bar))	Desalination rate	References
Commercial RO	0.997	99%	[46]
Two-stage RO model	15	100%	[47]
25%CA–0.05%CNT	4.3	96%	[48]
GO@RO	4.5	96%	[49]
TFN-GOQD/AP	2.5	98.4%	[50]
g-C ₃ N ₄	660	100%	[51]
GWFM	771	100%	[52]
BGR	1,020	98.1%	[53]
This work	857	100%	

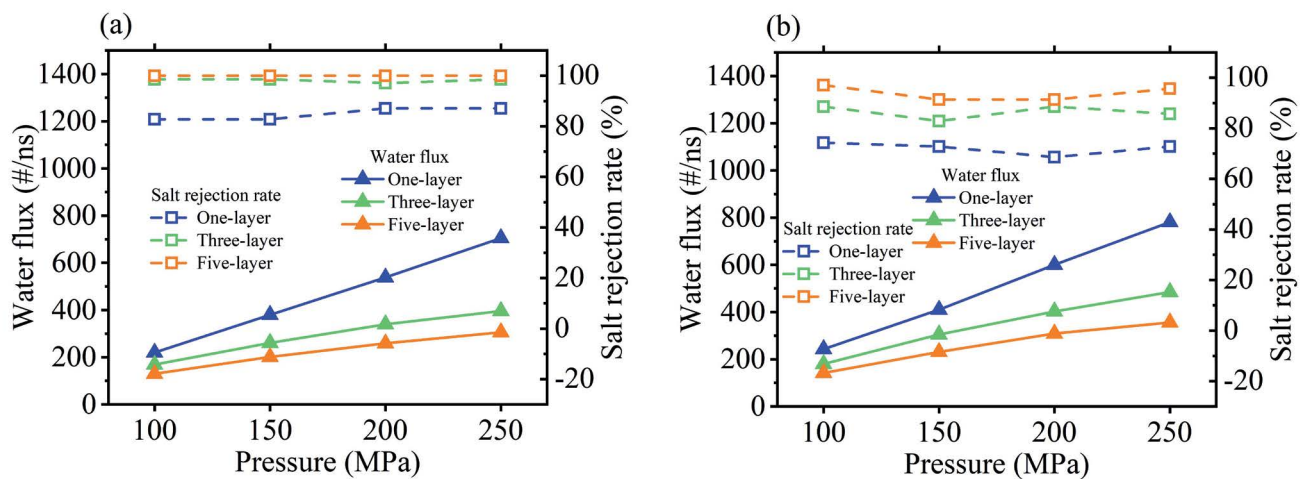


Fig. 6. Water flux and salt rejection rate of single-layer, three-layer or five-layer membrane changes with external force and slit size. The slits in the model are (a) 0.8 nm and (b) 0.9 nm.

the penetration of salts into the pore depth, hence reduce the tendency for scaling occurred [59]. The simulation duration of the Bernoulli effect desalination model is in nanoseconds level, which is very short. The sodium and chloride ions hydration diameter is very small, so they cannot pass through the pores during the simulation process, so other macromolecules certainly cannot pass through the pores and will not pollute and block the membrane. Therefore, there is no need to consider the problems of surfactants and other pollutants [15,60–62].

According to literature reports, centimeter-scale single-layer graphene films have been obtained by CVD growth on single-crystal copper foil [63], but larger-scale graphene films are currently difficult to produce. We compare the cost of graphene with other types of desalination membranes. The total cost of RO reported in Sarai Atab et al. [64] is 0.11 £/m³ when produce 24,000 m³/d of water from a feed salinity of 15,000 ppm with water quality of <400 ppm. Pearson et al. [65] reported that the general range of the RO operating cost of the City of Cape Coral North Plant, Florida, is 0.39–0.66 \$/m³. Electrodialysis has an energy requirement in the range of 0.4–4 kWh/m³ for brackish water (1,000–5,000 ppm) desalination [66]. The leveled

cost of water (LCOW) of osmotically assisted reverse osmosis (OARO) is in the range of 0.70–6.28 \$/m³, and the LCOW of batch-operated vacuum-air-gap membrane distillation (batch V-AGMD) is in the range of 1.74–2.77 \$/m³ [67]. The water cost of the hybrid system of multiple effect evaporation (MEE) and membrane distillation (MD) is found to be 2.05 \$/m³ [68]. von Eiff et al. [69] presents an advanced multi-stage flash crystallizer and the treatment cost is 1.17 \$/m³. The integration of the multi effect desalination (MED) with low temperature (60°C–95°C), medium temperature (165°C–200°C) and high temperature (370°C–530°C) solar collectors leads to water production costs of 2–3.6 \$/m³, 1.4–3.1 \$/m³ and 1.8–2.2 \$/m³ [70]. Al-Obaidi et al. [71] developed the hybrid multi effect distillation (MED) and RO system and the cost of the optimized hybrid MED + RO systems is 0.66 \$/m³. Carbon-based nanomaterials have great potential for efficient desalination due to their hydrophilicity, high water permeability, and high desalination rate, but their high production cost is considered to be the biggest obstacle to their industrialization, and it is estimated that the cost of graphene per gram is \$150–\$250 [72]. Although the cost of producing graphene is currently very high and there are many challenges in achieving desalination

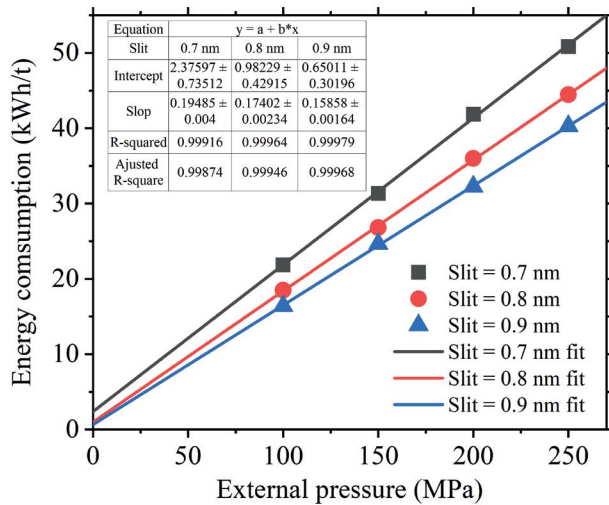


Fig. 7. Linear fitting diagram of energy consumption per ton for different slits under different external pressures.

applications similar to commercial RO membranes, but as demand increases and technology improves, the cost of graphene is expected to drop significantly and graphene has a promising future as a reverse osmosis membrane.

4. Conclusion

By applying the external force parallel to the membrane on the water molecules in one reservoir separated by the porous membrane, the directional movement of water molecules in the reservoir results in a reduction in pressure due to the Bernoulli effect, the water molecules move through the slits of membrane from the static reservoir to the dynamic reservoir. An efficient production of fresh water with high salt rejection rate could be achieved by the controllable slit in the membrane or the number of layers. It was found that both of the slit sizes in the membrane and the layers of the membrane have significant effects on water flux and salt rejection rate. For slits with high salt rejection rate, increasing the thickness has no effect on salt rejection rate, and the water flux would be reduced significantly. For slits with a low salt rejection rate, increasing the layers is beneficial to salt rejection rate, but the water flux would be still reduced. Therefore, factors such as slit size, thickness, and external force must be taken into consideration synthetically. The obtained results suggest a new type of desalination method and provide an idea for pumping system for separation and purification.

Declaration of competing interest

The authors declare that they have no known competing financial interests or personal relationships that could have appeared to influence the work reported in this paper.

Acknowledgments

The authors acknowledge the support of the National Natural Science Foundation of China (No. 51706157).

The numerical calculations in this paper have been done on the supercomputing system in the Supercomputing Center of Wuhan University.

References

- [1] M.A. Shannon, P.W. Bohn, M. Elimelech, J.G. Georgiadis, B.J. Mariñas, A.M. Mayes, Science and technology for water purification in the coming decades, *Nature*, 452 (2008) 301–310.
- [2] A. Taghizadeh, M. Taghizadeh, M. Jouyandeh, M.K. Yazdi, P. Zarrintaj, M.R. Saeb, E.C. Lima, V.K. Gupta, Conductive polymers in water treatment: a review, *J. Mol. Liq.*, 312 (2020) 113447, doi: 10.1016/j.molliq.2020.113447.
- [3] M.M. Mekonnen, A.Y. Hoekstra, Four billion people facing severe water scarcity, *Sci. Adv.*, 2 (2016) 1–6.
- [4] L.D. Tijning, Y.C. Woo, J.-S. Choi, S. Lee, S.-H. Kim, H.K. Shon, Fouling and its control in membrane distillation—a review, *J. Membr. Sci.*, 475 (2015) 215–244.
- [5] L.A. Hoover, W.A. Phillip, A. Tiraferri, N.Y. Yip, M. Elimelech, Forward with osmosis: emerging applications for greater sustainability, *Environ. Sci. Technol.*, 45 (2011) 9824–9830.
- [6] R. Xiong, C. Wei, Current status and technology trends of zero liquid discharge at coal chemical industry in China, *J. Water Process Eng.*, 19 (2017) 346–351.
- [7] G.P. Thiel, E.W. Tow, L.D. Banchik, H.W. Chung, J.H. Lienhard, Energy consumption in desalinating produced water from shale oil and gas extraction, *Desalination*, 366 (2015) 94–112.
- [8] A. Carati, M. Marino, D. Brogioli, Thermodynamic study of a distiller-electrochemical cell system for energy production from low temperature heat sources, *Energy*, 93 (2015) 984–993.
- [9] D. von Eiff, P.W. Wong, Y. Gao, S. Jeong, A.K. An, Technical and economic analysis of an advanced multi-stage flash crystallizer for the treatment of concentrated brine, *Desalination*, 503 (2021) 114925, doi: 10.1016/j.desal.2020.114925.
- [10] A.J. Toth, Modelling and optimisation of multi-stage flash distillation and reverse osmosis for desalination of saline process wastewater sources, *Membranes (Basel)*, 10 (2020) 1–18.
- [11] M.M. Alhazmy, Economic and thermal feasibility of multi stage flash desalination plant with brine-feed mixing and cooling, *Energy*, 76 (2014) 1029–1035.
- [12] A.M.K. El-Ghonemy, Performance test of a sea water multi-stage flash distillation plant: case study, *Alex. Eng. J.*, 57 (2018) 2401–2413.
- [13] M.M. Pendergast, E.M.V. Hoek, A review of water treatment membrane nanotechnologies, *Energy Environ. Sci.*, 4 (2011) 1946–1971.
- [14] A. Anand, B. Unnikrishnan, J.Y. Mao, H.J. Lin, C.C. Huang, Graphene-based nanofiltration membranes for improving salt rejection, water flux and antifouling—a review, *Desalination*, 429 (2018) 119–133.
- [15] Z. Zhang, F. Zhang, Z. Liu, G. Cheng, X. Wang, J. Ding, Molecular dynamics study on the reverse osmosis using multilayer porous graphene membranes, *Nanomaterials (Basel)*, 8 (2018) 1–13.
- [16] Y. Han, Z. Xu, C. Gao, Ultrathin graphene nanofiltration membrane for water purification, *Adv. Funct. Mater.*, 23 (2013) 3693–3700.
- [17] S.P. Surwade, S.N. Smirnov, I.V. Vlassioug, R.R. Unocic, G.M. Veith, S. Dai, S.M. Mahurin, Water desalination using nanoporous single-layer graphene, *Nat. Nanotechnol.*, 10 (2015) 459–464.
- [18] J.R. Werber, C.O. Osuji, M. Elimelech, Materials for next-generation desalination and water purification membranes, *Nat. Rev. Mater.*, 1 (2016) 1–16.
- [19] M. Xie, H.K. Shon, S.R. Gray, M. Elimelech, Membrane-based processes for wastewater nutrient recovery: technology, challenges, and future direction, *Water Res.*, 89 (2016) 210–221.
- [20] K. Choi, A. Droudian, R.M. Wyss, K.P. Schlichting, H.G. Park, Multifunctional wafer-scale graphene membranes for fast ultrafiltration and high permeation gas separation, *Sci. Adv.*, 4 (2018) 1–11.
- [21] J. Abraham, K.S. Vasu, C.D. Williams, K. Gopinadhan, Y. Su, C.T. Cherian, J. Dix, E. Prestat, S.J. Haigh, I.V. Grigorieva,

- P. Carbone, A.K. Geim, R.R. Nair, Tunable sieving of ions using graphene oxide membranes, *Nat. Nanotechnol.*, 12 (2017) 546–550.
- [22] Y. Yang, X. Yang, L. Liang, Y. Gao, H. Cheng, X. Li, M. Zou, R. Ma, Q. Yuan, X. Duan, Large-area graphene-nanomesh/carbon-nanotube hybrid membranes for ionic and molecular nanofiltration, *Science*, 364 (2019) 1057–1062.
- [23] A. Esfandiari, B. Radha, F.C. Wang, Q. Yang, S. Hu, S. Garaj, R.R. Nair, A.K. Geim, K. Gopinadhan, Size effect in ion transport through angstrom-scale slits, *Science*, 358 (2017) 1–3.
- [24] K. Celebi, J. Buchheim, R.M. Wyss, A. Droudian, P. Gasser, I. Shorubalko, J.I. Kye, C. Lee, H.G. Park, Ultimate permeation across atomically thin porous graphene, *Science*, 344 (2014) 289–292.
- [25] R.C. Rollings, A.T. Kuan, J.A. Golovchenko, Ion selectivity of graphene nanopores, *Nat. Commun.*, 7 (2016) 11408, doi: 10.1038/ncomms11408.
- [26] C.T. Nguyen, A. Beskok, Charged nanoporous graphene membranes for water desalination, *Phys. Chem. Chem. Phys.*, 21 (2019) 9483–9494.
- [27] J.A.L. Willcox, H.J. Kim, Molecular dynamics study of water flow across multiple layers of pristine, oxidized, and mixed regions of graphene oxide: effect of graphene oxide layer-to-layer distance, *J. Phys. Chem. C*, 121 (2017) 23659–23668.
- [28] W. Li, L. Zhang, X. Zhang, M. Zhang, T. Liu, S. Chen, Atomic insight into water and ion transport in 2D interlayer nanochannels of graphene oxide membranes: implication for desalination, *J. Membr. Sci.*, 596 (2020) 1–8.
- [29] K. Meidani, Z. Cao, A. Barati Farimani, Titanium carbide MXene for water desalination: a molecular dynamics study, *ACS Appl. Nano Mater.*, 4 (2021) 6145–6151.
- [30] M. Heiranian, A.B. Farimani, N.R. Aluru, Water desalination with a single-layer MoS₂ nanopore, *Nat. Commun.*, 6 (2015) 8616, doi: 10.1038/ncomms9616.
- [31] S. Chen, J. Ding, Q. Li, D. He, Y. Liu, L. Wang, Q. Lyu, M. Wang, Control one-dimensional length of rectangular pore on graphene membrane for better desalination performance, *Nanotechnology*, 33 (2022) 1–11.
- [32] Z. Li, Q. Han, Y. Qiu, Field-enhanced water transport in sub-nanometer graphene nanopores, *Desalination*, 528 (2022) 115610, doi: 10.1016/j.desal.2022.115610.
- [33] V. Mortazavi, A. Moosavi, A. Nouri-Borujerdi, Enhancing water desalination in graphene-based membranes via an oscillating electric field, *Desalination*, 495 (2020) 114672, doi: 10.1016/j.desal.2020.114672.
- [34] T.A. Beu, Molecular dynamics simulations of ion transport through carbon nanotubes. I. Influence of geometry, ion specificity, and many-body interactions, *J. Chem. Phys.*, 132 (2010) 1–16.
- [35] H.T. Kieu, B. Liu, K. Zhou, A.W.-K. Law, Pressure-driven water permeation through multilayer graphene nanosheets, *Phys. Status Solidi B*, 254 (2017) 1–10.
- [36] S. Plimpton, Fast parallel algorithms for short-range molecular dynamics, *J. Comput. Phys.*, 117 (1995) 1–19.
- [37] S. Nosé, A unified formulation of the constant temperature molecular dynamics methods, *J. Chem. Phys.*, 81 (1984) 511–519.
- [38] W.G. Hoover, Canonical dynamics: equilibrium phase-space distributions, *Phys. Rev. A*, 31 (1985) 1695–1697.
- [39] V. Mortazavi, A. Moosavi, A. Nouri-Borujerdi, Enhancing water desalination in graphene-based membranes via an oscillating electric field, *Desalination*, 495 (2020) 1–11.
- [40] J.P. Ryckaert, G. Ciccoliti, H.J.C. Berendsen, Numerical integration of the cartesian equations of motion of a system with constraints: molecular dynamics of *n*-alkanes, *J. Comput. Phys.*, 23 (1977) 327–341.
- [41] C.L. Kong, Combining rules for intermolecular potential parameters. II. Rules for the Lennard–Jones (12–6) potential and the Morse potential, *J. Chem. Phys.*, 59 (1973) 2464–2467.
- [42] R.W. Hockney, J.W. Eastwood, *Computer Simulation Using Particles*, CRC Press, Boca Raton, 1988.
- [43] S.M. Ghodsi, S. Sharifi-Asl, P. Rehak, P. Král, C.M. Megaridis, R. Shahbazian-Yassar, T. Shokuhfar, Assessment of pressure and density of confined water in graphene liquid cells, *Adv. Mater. Interfaces*, 7 (2020) 1–10.
- [44] S. Koneshan, J.C. Rasaiah, R.M. Lynden-Bell, S.H. Lee, Solvent structure, dynamics, and ion mobility in aqueous solutions at 25°C, *J. Phys. Chem. B*, 102 (1998) 4193–4204.
- [45] S. Sahu, M. Zwolak, Ionic selectivity and filtration from fragmented dehydration in multilayer graphene nanopores, *Nanoscale*, 9 (2017) 11424–11428.
- [46] S.R. Osipi, A.R. Secchi, C.P. Borges, Cost assessment and retro-techno-economic analysis of desalination technologies in onshore produced water treatment, *Desalination*, 430 (2018) 107–119.
- [47] Q.J. Wei, R.K. McGovern, J.H. Lienhard V, Saving energy with an optimized two-stage reverse osmosis system, *Environ. Sci. Water Res. Technol.*, 3 (2017) 659–670.
- [48] L.A.N. El-Din, A. El-Gendi, N. Ismail, K.A. Abed, A.I. Ahmed, Evaluation of cellulose acetate membrane with carbon nanotubes additives, *J. Ind. Eng. Chem.*, 26 (2015) 259–264.
- [49] M.Y. Ashfaq, M.A. Al-Ghouthi, N. Zouari, Functionalization of reverse osmosis membrane with graphene oxide to reduce both membrane scaling and biofouling, *Carbon*, 166 (2020) 374–387.
- [50] S. Li, B. Gao, Y. Wang, B. Jin, Q. Yue, Z. Wang, Antibacterial thin film nanocomposite reverse osmosis membrane by doping silver phosphate loaded graphene oxide quantum dots in polyamide layer, *Desalination*, 464 (2019) 94–104.
- [51] Y. Liu, Z. Cheng, M. Song, L. Jiang, G. Fu, L. Liu, J. Li, Molecular dynamics simulation-directed rational design of nanoporous graphitic carbon nitride membranes for water desalination, *J. Membr. Sci.*, 620 (2021) 118869, doi: 10.1016/j.memsci.2020.118869.
- [52] T. Liu, J. Lyv, Y. Xu, C. Zheng, Y. Liu, R. Fu, L. Liang, J. Wu, Z. Zhang, Graphene-based woven filter membrane with excellent strength and efficiency for water desalination, *Desalination*, 533 (2022) 115775, doi: 10.1016/j.desal.2022.115775.
- [53] Q. Shi, H. Gao, Y. Zhang, Z. Meng, D. Rao, J. Su, Y. Liu, Y. Wang, R. Lu, Bilayer graphene with ripples for reverse osmosis desalination, *Carbon*, 136 (2018) 21–27.
- [54] E.Y.M. Ang, T.Y. Ng, J. Yeo, Z. Liu, K.R. Geethalakshmi, Free-standing graphene slit membrane for enhanced desalination, *Carbon*, 110 (2016) 350–355.
- [55] X. Jia, J. Klemeš, P. Varbanov, S. Wan Alwi, Analyzing the energy consumption, GHG emission, and cost of seawater desalination in China, *Energies*, 12 (2019) 1–16.
- [56] D. Zarzo, D. Prats, Desalination and energy consumption. What can we expect in the near future?, *Desalination*, 427 (2018) 1–9.
- [57] K. Park, J. Kim, D.R. Yang, S. Hong, Towards a low-energy seawater reverse osmosis desalination plant: a review and theoretical analysis for future directions, *J. Membr. Sci.*, 595 (2020) 1–47.
- [58] F. Leon, A. Ramos, S.O. Perez-Baez, Optimization of energy efficiency, operation costs, carbon footprint and ecological footprint with reverse osmosis membranes in seawater desalination plants, *Membranes (Basel)*, 11 (2021) 1–18.
- [59] P. Daraei, S.S. Madaeni, N. Ghaemi, M.A. Khadivi, B. Astinchap, R. Moradian, Enhancing antifouling capability of PES membrane via mixing with various types of polymer modified multi-walled carbon nanotube, *J. Membr. Sci.*, 444 (2013) 184–191.
- [60] M. Dahanayaka, B. Liu, N. Srikanth, K. Zhou, Ionised graphene oxide membranes for seawater desalination, *Desalination*, 496 (2020) 114637, doi: 10.1016/j.desal.2020.114637.
- [61] M. Ali Abdol, S. Sadeghzadeh, M. Jalaly, M. Mahdi Khatibi, On the desalination performance of multi-layer graphene membranes: a molecular dynamics study, *Comput. Mater. Sci.*, 191 (2021) 110335, doi: 10.1016/j.commatsci.2021.110335.
- [62] Y. Zhang, T. Fang, Q. Hou, Z. Li, Y. Yan, Water desalination of a new three-dimensional covalent organic framework: a molecular dynamics simulation study, *Phys. Chem. Chem. Phys.*, 22 (2020) 16978–16984.
- [63] M. Wang, D. Luo, B. Wang, R.S. Ruoff, Synthesis of large-area single-crystal graphene, *Trends Chem.*, 3 (2021) 15–33.

- [64] M. Sarai Atab, A.J. Smallbone, A.P. Roskilly, An operational and economic study of a reverse osmosis desalination system for potable water and land irrigation, *Desalination*, 397 (2016) 174–184.
- [65] J.L. Pearson, P.R. Michael, N. Ghaffour, T.M. Missimer, Economics and energy consumption of brackish water reverse osmosis desalination: innovations and impacts of feedwater quality, *Membranes (Basel)*, 11 (2021) 1–21.
- [66] N. Mir, Y. Bicer, Integration of electrodialysis with renewable energy sources for sustainable freshwater production: a review, *J. Environ. Manage.*, 289 (2021) 112496, doi: 10.1016/j.jenvman.2021.112496.
- [67] Z. Zhang, A.A. Atia, J.A. Andrés-Mañas, G. Zaragoza, V. Fthenakis, Comparative techno-economic assessment of osmotically-assisted reverse osmosis and batch-operated vacuum-air-gap membrane distillation for high-salinity water desalination, *Desalination*, 532 (2022) 115737, doi: 10.1016/j.desal.2022.115737.
- [68] E. Ali, J. Orfi, H. AlAnsary, S. Soukane, H. Elcik, A. Alpatova, N. Ghaffour, Cost analysis of multiple effect evaporation and membrane distillation hybrid desalination system, *Desalination*, 517 (2021) 115258, doi: 10.1016/j.desal.2021.115258.
- [69] D. von Eiff, P.W. Wong, Y. Gao, S. Jeong, A.K. An, Technical and economic analysis of an advanced multi-stage flash crystallizer for the treatment of concentrated brine, *Desalination*, 503 (2021) 114925, doi: 10.1016/j.desal.2020.114925.
- [70] I. Baniasad Askari, M. Ameri, A techno-economic review of multi effect desalination systems integrated with different solar thermal sources, *Appl. Therm. Eng.*, 185 (2021) 116323, doi: 10.1016/j.applthermaleng.2020.116323.
- [71] M.A. Al-Obaidi, G. Filippini, F. Manenti, I.M. Mujtaba, Cost evaluation and optimisation of hybrid multi effect distillation and reverse osmosis system for seawater desalination, *Desalination*, 456 (2019) 136–149.
- [72] G.M. de Costa, C.M. Hussain, Ethical, legal, social and economics issues of graphene, *Compr. Anal. Chem.*, 91 (2020) 263–279.

Supporting information

S1. Single-layer graphene model with slit of 0.6 nm

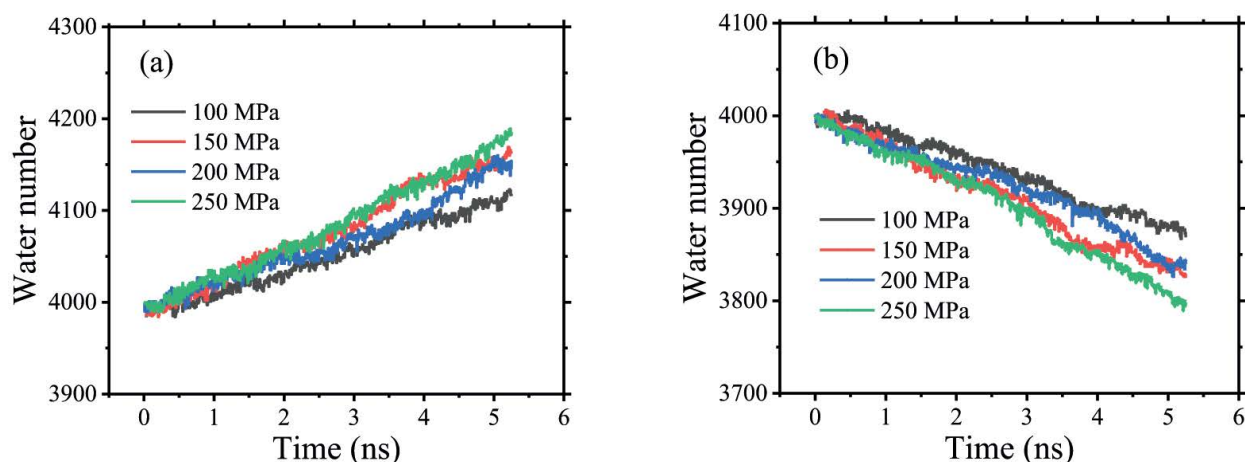


Fig. S1. Under different external force, the number of water molecules in (a) the upper dynamic reservoir and (b) the lower static reservoir changes with the simulation time.

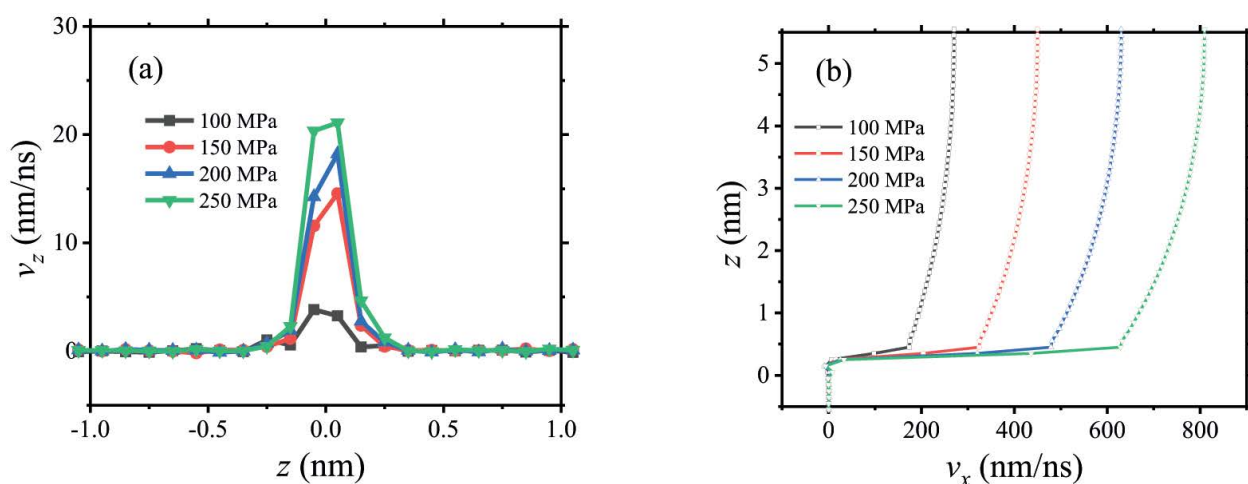


Fig. S2. Along the z-axis in the model, the velocity component of water molecules in (a) the z-direction and (b) the x-direction.

S2. Single-layer graphene model with slit of 0.8 nm

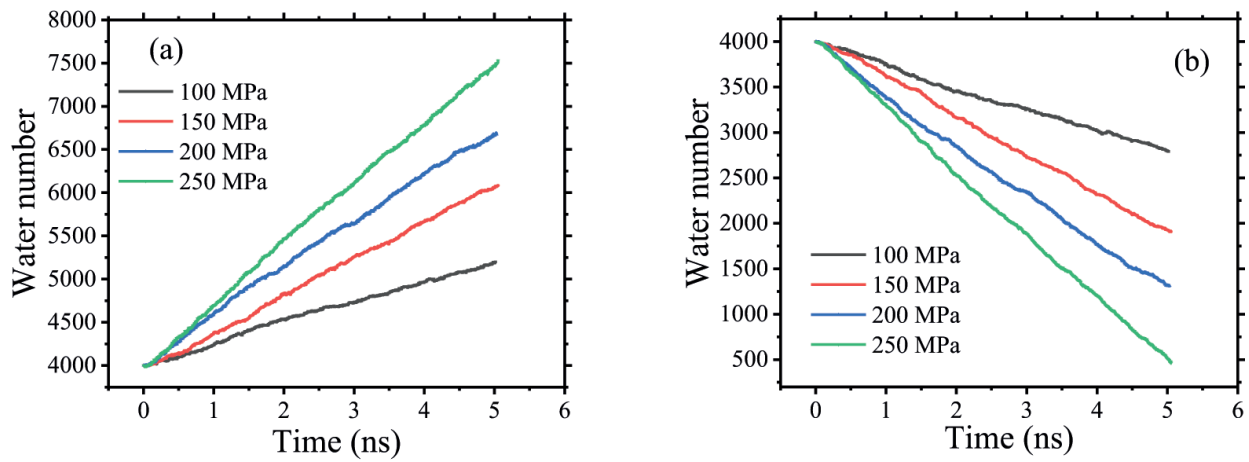


Fig. S3. Under different external force, the number of water molecules in (a) the upper dynamic reservoir and (b) the lower static reservoir changes with the simulation time.

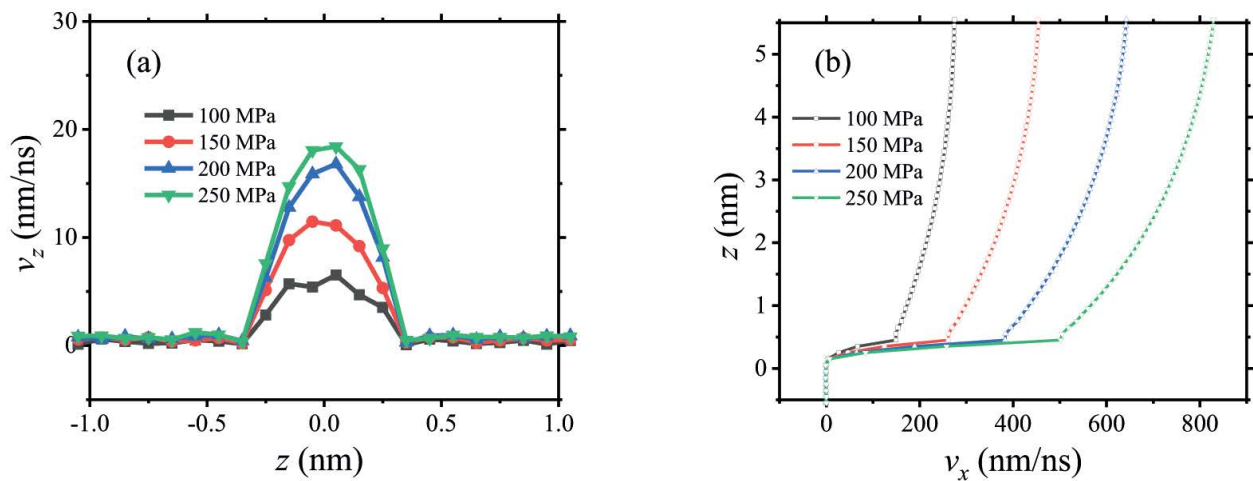


Fig. S4. Along the z-axis in the model, the velocity component of water molecules in (a) the z-direction and (b) the x-direction.

S3. Single-layer graphene model with slit of 0.9 nm

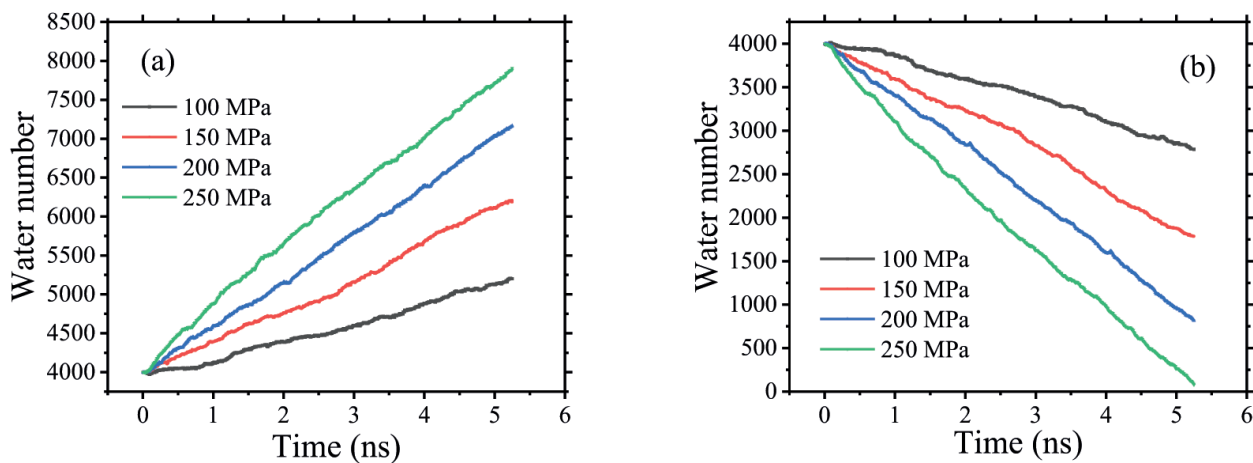


Fig. S5. Under different external force, the number of water molecules in (a) the upper dynamic reservoir and (b) the lower static reservoir changes with the simulation time.

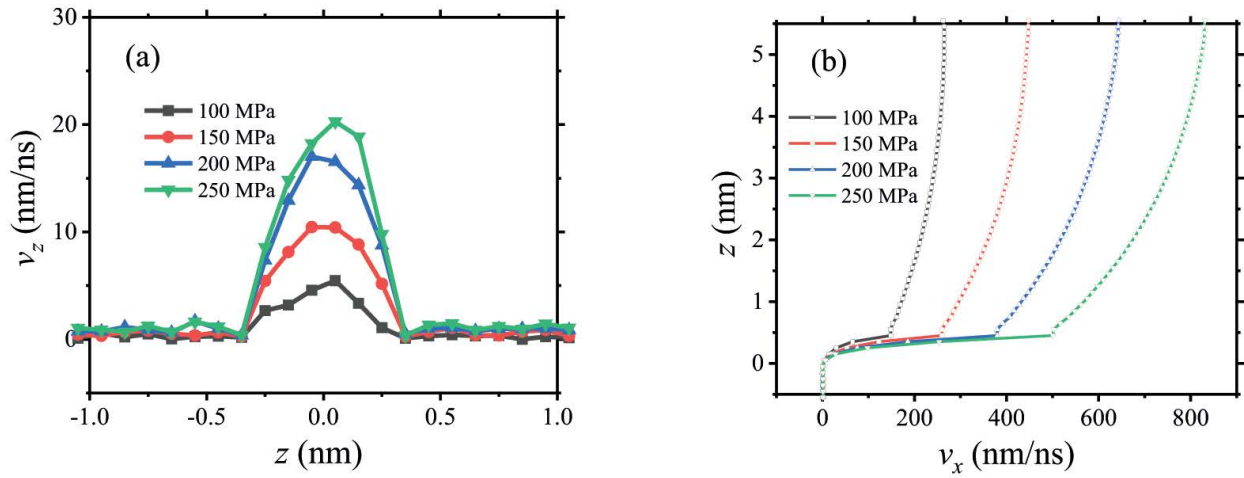


Fig. S6. Along the z -axis in the model, the velocity component of water molecules in (a) the z -direction and (b) the x -direction.

S4. Three-layer graphene model with slit of 0.8 nm

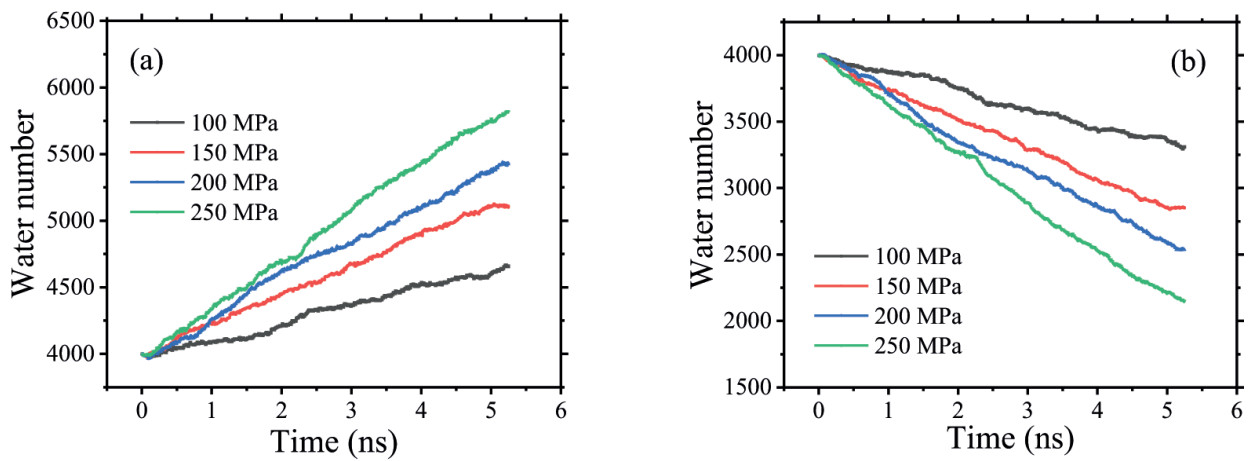


Fig. S7. Under different external force, the number of water molecules in (a) the upper dynamic reservoir and (b) the lower static reservoir changes with the simulation time.

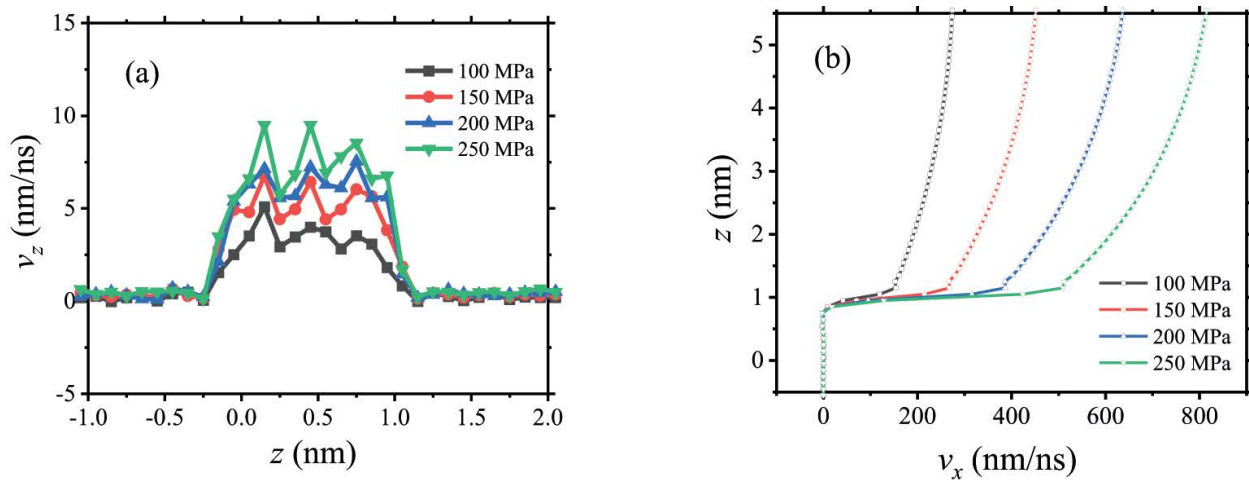


Fig. S8. Along the z -axis in the model, the velocity component of water molecules in (a) the z -direction and (b) the x -direction.

S5. Three-layer graphene model with slit of 0.9 nm

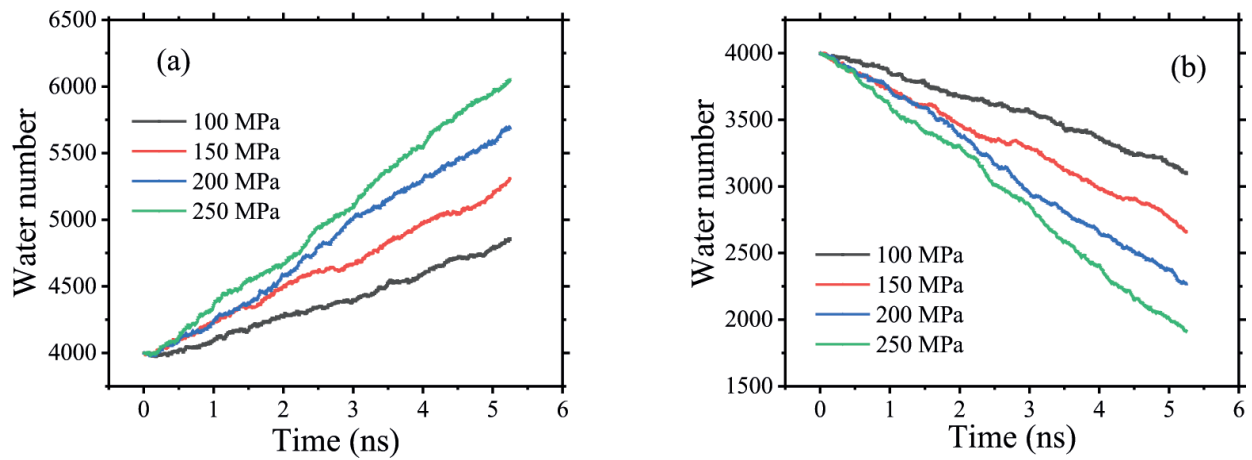


Fig. S9. Under different external force, the number of water molecules in (a) the upper dynamic reservoir and (b) the lower static reservoir changes with the simulation time.

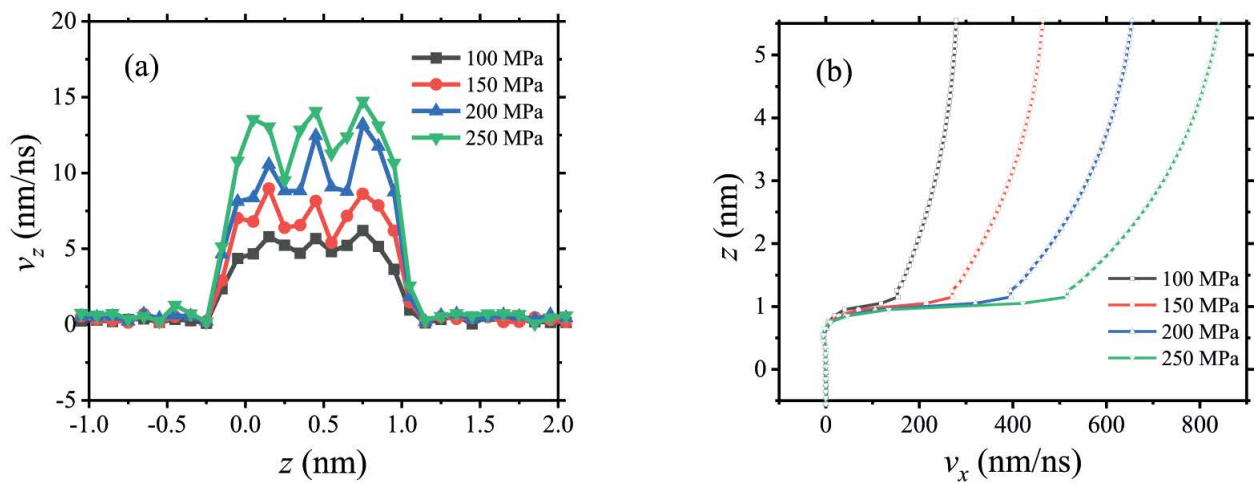


Fig. S10. Along the z-axis in the model, the velocity component of water molecules in (a) the z-direction and (b) the x-direction.

S6. Five-layer graphene model with slit of 0.8 nm

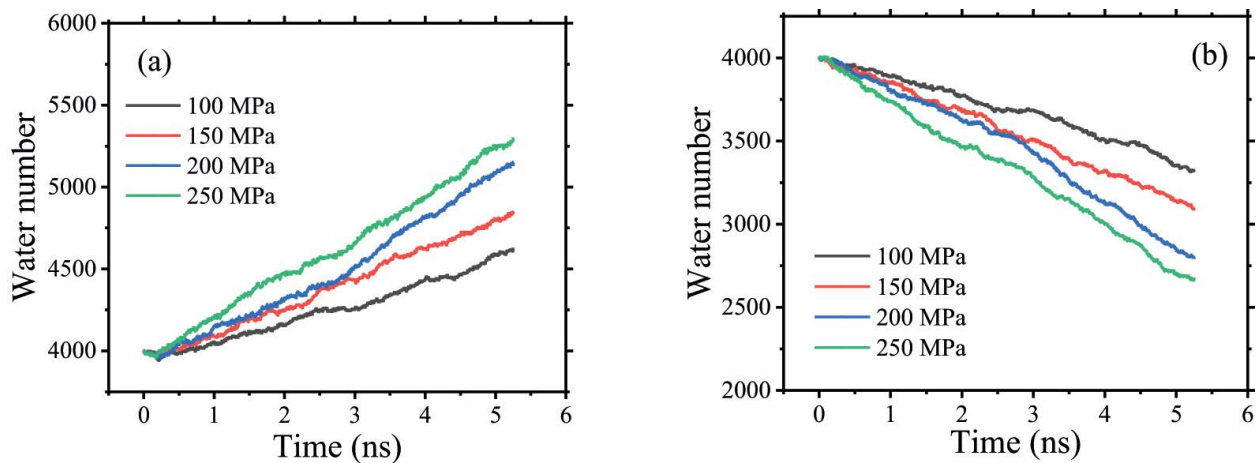


Fig. S11. Under different external force, the number of water molecules in (a) the upper dynamic reservoir and (b) the lower static reservoir changes with the simulation time.

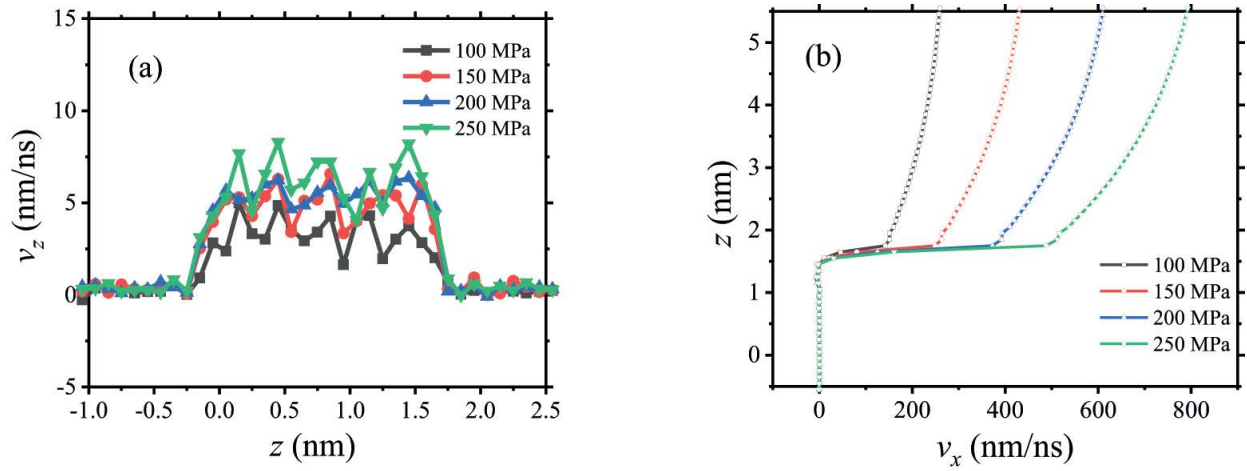


Fig. S12. Along the z -axis in the model, the velocity component of water molecules in (a) the z -direction and (b) the x -direction.

S7. Five-layer graphene model with slit of 0.9 nm

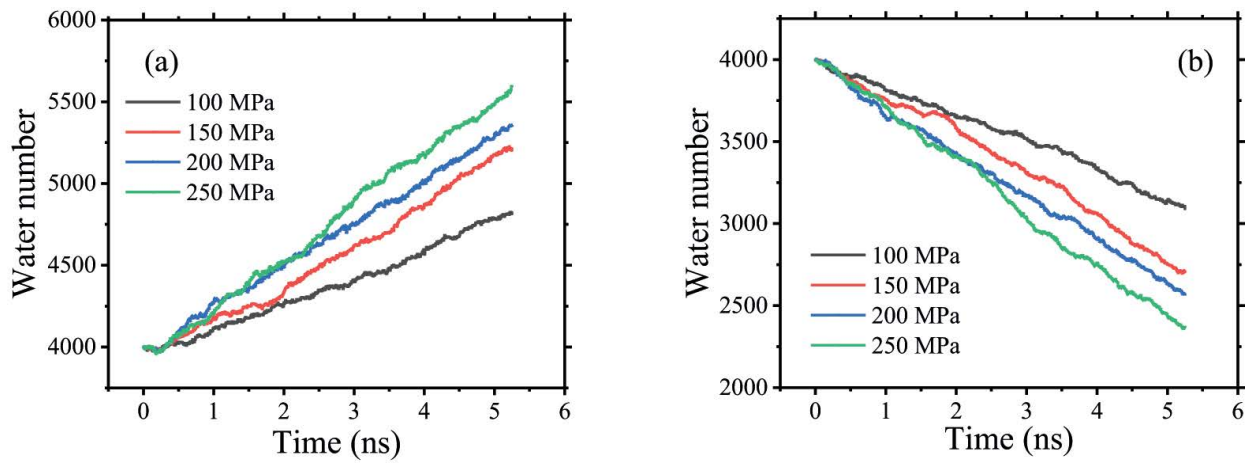


Fig. S13. Under different external force, the number of water molecules in (a) the upper dynamic reservoir and (b) the lower static reservoir changes with the simulation time.

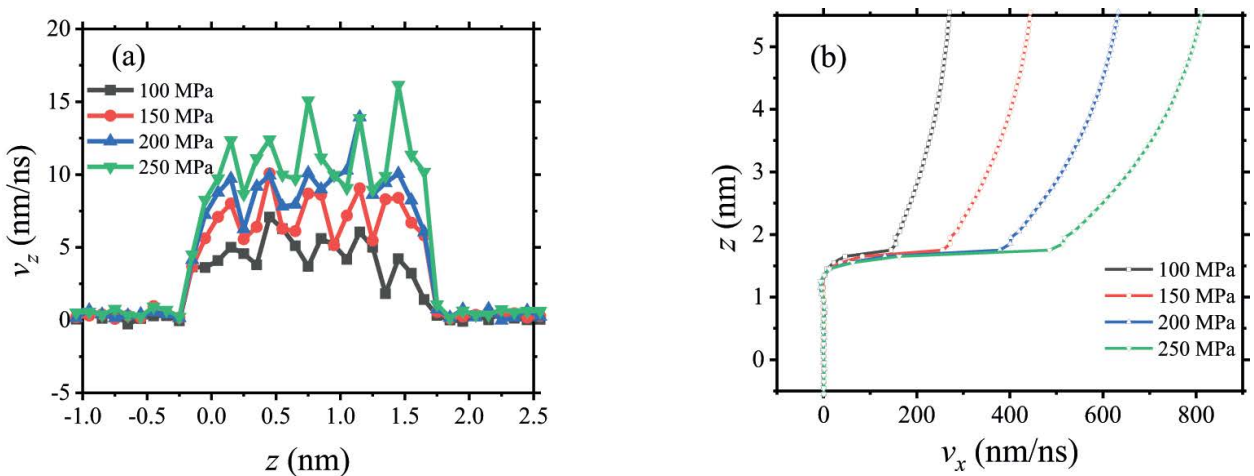


Fig. S14. Along the z -axis in the model, the velocity component of water molecules in (a) the z -direction and (b) the x -direction.